Proceedings of the XIth International Congress and Exposition
June 2-5, 2008 Orlando, Florida USA

A New Microdevice for SI-Traceable Forces in Atomic Force Microscopy

Gregory W. Vogl, Jason J. Gorman, Gordon A. Shaw, and Jon R. Pratt
Manufacturing Engineering Laboratory
National Institute of Standards and Technology
Gaithersburg, Maryland 20899-8221
Email: gvogl@nist.gov

ABSTRACT

A new self-excited micro-oscillator is proposed as a velocity standard for dissemination of nanonewton-level forces that are traceable to the International System of Units (SI). The microfabricated oscillator is top-coated with magnetic thin films and closely surrounded with conductive microwires to enable both magnetic sensing and actuation. An analog control system will keep the actuation side of the device oscillating sinusoidally with a frequency up to 200 kHz and a nanometer-level amplitude that is fairly insensitive to the quality factor. Consequently, the device can be calibrated as a velocity standard in air and used in ultra-high vacuum with a velocity shift of less than one percent. Because of the nanometer-level oscillation amplitude, the microdevice could be used to probe capacitance gradients near tips of cantilevers used for atomic force microscopy (AFM). Hence, the calibrated micro-oscillator could be used with electrostatic forces to calibrate AFM cantilevers as SI-traceable force transducers for fundamental metrology of electrical and mechanical nanoscale quantities.

Introduction

Since the development of AFM [1], atomic resolution was achieved over a decade ago [2,3] and the method has been used to characterize electrical, magnetic, and mechanical properties of materials. However, commercial AFM suffers from a lack of accurate force measurements because there is presently no method to disseminate SI-traceable nanonewton-level forces to most AFM users. This situation concerns AFM users who need to measure and control the small forces between an AFM cantilever tip and the substrate surface, e.g., in single-molecule force spectroscopy [4,5]. Traceability is also needed to compare AFM force measurements to those made by optical tweezers and other methods. Otherwise, the reliable fabrication and testing of future microscale devices may be in doubt.

Currently, no method exists for the SI-traceable calibration of AFM cantilevers in various AFM environments. Tip-sample forces are usually calculated by Hooke's law ($F = kx$) with an estimated cantilever stiffness (k) and a measured tip deflection (x). For example, dynamic methods for estimation of the stiffness usually rely on the thermal noise spectrum [6,7], the resonant frequency shift with added mass [8], or the resonant frequency with knowledge of the cantilever density and dimensions [9]. While possibly being efficient or available for *in situ* calibration, these methods do not yield SI-traceable cantilever stiffnesses because of the lack of SI-traceable forces. Alternatively, traceable forces from calibrated masses [10] or reference cantilevers calibrated with an electrostatic force balance [11] may be used for static cantilever calibrations, but these methods are usually not efficient or available for *in situ* calibration, particularly in extreme cryogenic environments.

Proposed Device

A new self-excited oscillator is proposed to allow SI-traceable calibrations of AFM cantilevers in several environments. The proposed micro-oscillator is composed of a sensing side and an actuation side, as outlined in Fig. 1(a). The actuation side is attached to a rigid substrate (not shown) through two flexures, while the sensing side is attached to the actuation side by a thin flexure. Magnetic sensing and actuation are possible because both sides of the device are top-coated with magnetic thin films of nickel and closely surrounded by chrome/gold microwires. Accordingly, the rotational velocity of the sensing side is observed in the sensing current according to Faraday's law of magnetic induction, while the interaction of the actuation current with the magnetic thin film produces a torque on the actuation side.

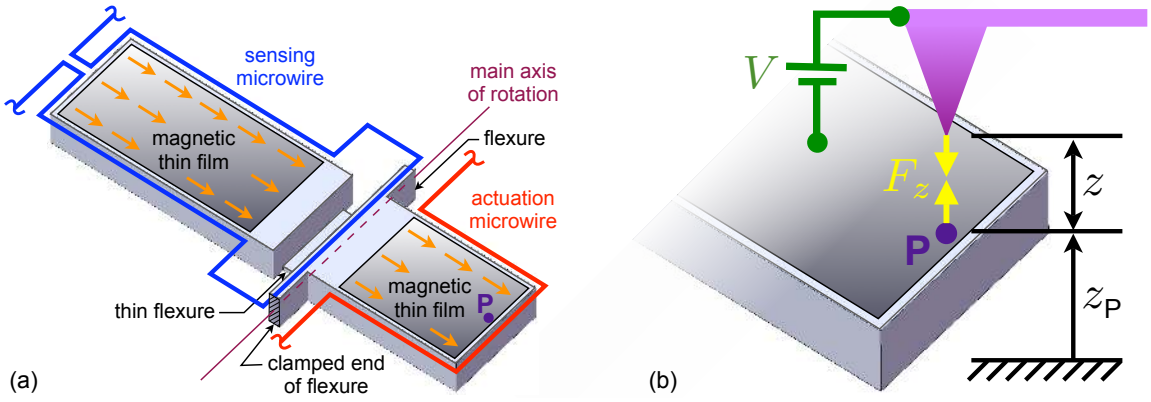

Figure 1: (a) Proposed micro-oscillator that is composed of a sensing side (left) and an actuator side (right) that are top-coated in magnetic thin films, which are magnetized lengthwise and closely surrounded by microwires, and (b) a schematic of the actuation side of the device during an AFM cantilever calibration. The device is not to scale.

The device modeling, control, and microfabriction will be described in this paper. However, the potential use of the micro-oscillator for traceable AFM cantilever calibrations is explained first.

Device as Velocity Standard

During calibration of an AFM cantilever, the small forces applied to the cantilever will be non-contact and electrostatic in nature. As seen in Fig. 1(b), the cantilever tip is brought very close above point P, with a vertical separation z between the tip and the device. A known voltage V is then applied across the "capacitor", which is the cantilever-device system with capacitance C. Consequently, a net vertical electrostatic force exists with a magnitude F_z that is defined by

$$F_z = \frac{1}{2}\left|\frac{dC}{dz}\right|V^2 \tag{1}$$

Hence, once the capacitance gradient dC/dz is determined, the electrostatic force F_z will be known. In fact, the microdevice will be magnetically oscillated and the resulting vibration at point P will be calibrated and used to determine the needed capacitance gradient dC/dz.

Understanding how the velocity of point P is used to determine the capacitance gradient begins by noting that the charge q and the potential difference V for a capacitor are proportional to each other through the capacitance; that is,

$$q = CV \tag{2}$$

Hence, the displacement current $i = dq/dt$ is

$$i = \frac{d}{dt}(CV) \tag{3}$$

Because the capacitance C changes only with the gap distance z, the current becomes

$$i = \frac{dC}{dz}\frac{dz}{dt}V_0 \tag{4}$$

when the gap distance varies with time t while the voltage remains constant at V_0.

Next, we assume that the vibration frequency of the device is far away from all resonant frequencies of the AFM cantilever. Consequently, the cantilever will not be excited and can be regarded as fixed during the device oscillation, which means that

$$\frac{dz}{dt} = -\frac{dz_{\mathrm{P}}}{dt} \tag{5}$$

by inspection of Fig. 1(b). Furthermore, if point P oscillates with a sufficiently small amplitude such that the capacitance gradient is essentially constant over the oscillation range, then the root mean square (rms) of the current becomes

$$i_{\mathrm{rms}} = \left|\frac{dC}{dz}\right| |V_0| \left(\frac{dz_{\mathrm{P}}}{dt}\right)_{\mathrm{rms}} \tag{6}$$

according to Eqn. (4). Finally, we solve for the capacitance gradient and substitute the result into Eqn. (1) to obtain

$$F_z = \frac{i_{\mathrm{rms}}|V_0|}{2\left(\dot{z}_{\mathrm{P}}\right)_{\mathrm{rms}}} \tag{7}$$

where the overdot represents differentiation with respect to time. Equation (7) reveals that if a traceable voltage V_0, rms current i_{rms}, and velocity of point P are measured during calibration of an AFM cantilever, then the electrostatic force F_z is known with SI traceability. Moreover, if the velocity of point P is the same before and during AFM cantilever calibrations, then the microdevice can be calibrated as a velocity standard for subsequent cantilever calibrations.

This approach is valid because micronewton- and nanonewton-level forces may be achieved with an electrostatic force balance through the SI-traceable electrical units that are linked to the Josephson and quantized Hall effects [12]. Furthermore, the use of a micro-oscillator for the application of traceable electrostatic forces has already been achieved by Cumpson and Hedley [13]. Their micro-oscillator was calibrated *in situ* with Doppler velocimetry and, along with the necessary electrical and distance measurements, the device spring constant was determined. Subsequently, the device was used as a reference artifact for cantilever-on-reference calibrations. In contrast, Chung et al. [14] applied SI-traceable electrostatic forces directly to an indentation force sensor to be calibrated.

Approximate Model

Before controlling the device for use as a velocity standard, the system is modeled as a two-degree-of-freedom system. The sensing and actuation masses are treated as rigid bodies that rotate with angles ψ and θ about one fixed central axis, as seen in Fig. 2. The rotational inertias of the sensing and actuation sides about the central axis are I_{s} and I_{a}, respectively. The torsional stiffness of the actuation side is κ_{a}, while the torsional stiffness of the sensing side is κ_{s} relative to the actuation side. Consequently, the fundamental frequencies used for the simplified model are ω_{s} and ω_{a} and are defined by $\omega_{\mathrm{s}}^2 = \kappa_{\mathrm{s}}/I_{\mathrm{s}}$ and $\omega_{\mathrm{a}}^2 = \kappa_{\mathrm{a}}/I_{\mathrm{a}}$, respectively.

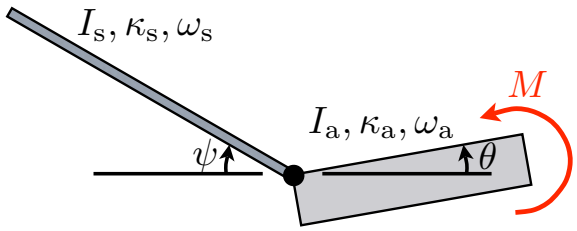

Figure 2: Approximate model of proposed micro-oscillator.

For a net applied moment M on the actuation side, as seen in Fig. 2, the rotational form of Newton's second law yields the two equations of motion,

$$I_{\mathrm{s}}\ddot{\psi} + 2\zeta_{\mathrm{s}} I_{\mathrm{s}}\omega_{\mathrm{s}}\dot{\psi} + \kappa_{\mathrm{s}}(\theta + \psi) = 0 \tag{8a}$$

$$I_{\mathrm{a}}\ddot{\theta} + 2\zeta_{\mathrm{a}} I_{\mathrm{a}}\omega_{\mathrm{a}}\dot{\theta} + \kappa_{\mathrm{s}}(\theta + \psi) + \kappa_{\mathrm{a}}\theta = M \tag{8b}$$

where linear damping has been assumed to exist with the viscous damping factors ζ_{s} and ζ_{a} for the sensing and actuation sides, respectively.

We nondimensionalize time as $\bar{t} = \omega_{\mathrm{s}} t$ and subsequently nondimensionalize Eqns. (8) to obtain

$$\psi'' + 2\zeta_{\mathrm{s}}\psi' + \psi + \theta = 0 \tag{9a}$$

$$\lambda\theta'' + 2\zeta_{\mathrm{a}}\lambda\beta\theta' + (1 + \lambda\beta^2)\theta + \psi = \tau \tag{9b}$$

where the prime represents differentiation with respect to the nondimensional time $\bar{t}$, $\lambda = I_\mathrm{a}/I_\mathrm{s}$, $\beta = \omega_\mathrm{a}/\omega_\mathrm{s}$, and $\tau = M/\kappa_\mathrm{s}$. We note that $\lambda\beta^2 = \kappa_\mathrm{a}/\kappa_\mathrm{s}$ and represents the relative torsional stiffnesses of the oscillator sides. Equations 9 are used for the system analysis and control described herein.

Design Goals

The system parameters (λ and β) and forcing function (τ) for Eqns. (9) must be chosen to achieve three goals regarding the system oscillation:

1. The sensing angle ψ is generally much larger than the actuation angle θ.
2. The actuation angle θ approaches a sinusoidal limit cycle.
3. The sinusoidal limit cycle for θ is fairly insensitive to the quality factor $Q = 1/2\zeta_\mathrm{s}$.

Goal 1 will give us a "mechanical advantage" to boost the sensing current and consequently decrease the gain required to create the actuation current.

Goal 2 will ensure a precise sinusoidal motion that is desired for calibration purposes. Firstly, we could measure the rms signal and simply determine its amplitude if needed. Secondly, the device should operate with only one frequency component to minimize the chances of exciting an AFM cantilever during calibration.

Goal 3 ensures a reliable motion despite possible changes in Q. Therefore, the oscillator could be calibrated as a velocity standard *ex situ* (like in air) and then used with a minor shift in velocity for AFM cantilever calibrations *in situ* (like in vacuum). The enabling of velocity calibration *ex situ* would be an advancement over the *in situ* velocity calibration performed by Cumpson and Hedley [13].

Controlled System

The development of the controlled system shows that the three goals can be achieved with a system that asymptotically approaches a sinusoidal limit cycle [15]; that is,

$$\psi \to A_\psi \cos(\bar{\omega}\bar{t} + \varphi_\psi) \tag{10a}$$
$$\theta \to A_\theta \cos(\bar{\omega}\bar{t} + \varphi_\theta) \tag{10b}$$

as $\bar{t} \to \infty$, in which A_ψ and A_θ are the amplitudes, φ_ψ and φ_θ are the phases that depend on the initial conditions, and $\bar{\omega}$ is the nondimensional limit cycle frequency. The amplitude A_ψ of sensing motion should be much larger (Goal 1) than the amplitude A_θ of the sinusoidal (Goal 2) actuation motion. Also, the system must be controlled so that A_θ remains fairly constant with Q (Goal 3).

Equations (9) are augmented with control equations to achieve the three goals. One system that achieves a sinusoidal limit cycle for θ (Goal 2) with $A_\psi \gg A_\theta$ (Goal 1) and $A_\theta \not\approx f(Q)$ (Goal 3) is

$$\psi'' + 2\zeta_\mathrm{s}\psi' + \psi + \theta = 0 \tag{11a}$$
$$\lambda\theta'' + 2\zeta_\mathrm{a}\lambda\beta\theta' + (1 + \lambda\beta^2)\theta + \psi = -\eta\psi' \tag{11b}$$
$$\Psi'' + 2\zeta_\mathrm{f}\omega_\mathrm{f}\Psi' + \omega_\mathrm{f}^2\Psi = \omega_\mathrm{f}^2(\psi')^2 \tag{11c}$$
$$\eta = \epsilon\,(1 - \alpha\Psi) \tag{11d}$$
$$\nu\epsilon' + \epsilon = \eta + \frac{1}{\eta} \tag{11e}$$

where ζ_f, ω_f, α, and ν are nondimensional control parameters, and the nondimensional variables η, ϵ, and Ψ change with time to achieve the desired system response [15]. Physically, the sensing current is amplified to produce the actuation current and hence the magnetically-induced actuation torque. Nondimensionally, this action is seen in the right-hand side of Eqn. (11b), where ψ' is multipled by $-\eta$ to produce the nondimensional torque. The feedback gain η is defined by Eqn. (11d) and depends on ϵ and Ψ. The gain ϵ adapts itself through the first-order Butterworth filter in Eqn. (11e)

to achieve η such that $A_\theta \not\approx f(Q)$ (Goal 3). Also, the signal Ψ is the filtered version of $(\psi')^2$ from the second-order Butterworth filter in Eqn. (11c) and is used to produce a sinusoidal limit cycle (Goal 2).

Finally, this system causes motion that satisfies the three goals when the system is either "stiff" ($\beta \gg 1$ and $\lambda\beta^2 \gg 1$) or "heavy" ($\beta \ll 1$ and $\lambda \gg 1$). By definition, a system is "stiff" when $\omega_\mathrm{a} \gg \omega_\mathrm{s}$ and $\kappa_\mathrm{a} \gg \kappa_\mathrm{s}$ or "heavy" when $\omega_\mathrm{a} \ll \omega_\mathrm{s}$ and $I_\mathrm{a} \gg I_\mathrm{s}$. For these two cases, the sensing side resonates while the actuation side is far away from resonance, due to the resonant frequency ω_a of the actuation side being much larger ($\beta \gg 1$) or smaller ($\beta \ll 1$) than the resonant frequency ω_s of the sensing side. Hence, the motion of the actuation side is either stiffness-dominated ($\kappa_\mathrm{a} \gg \kappa_\mathrm{s}$) or inertia-dominated ($I_\mathrm{a} \gg I_\mathrm{s}$) while the sensing side vibrates near resonance [15].

Theoretical Results

Figure 3 shows the system responses for two different cases in which Q jumps from 1000 to 100 at approximately the 2000th cycle. Before the rapid decrease in Q, the amplitudes and gains in both cases approach steady values. However, after the change in Q, the gain ϵ adjusts to maintain $A_\theta \approx 0.0001$ for the limit cycle, while ψ is allowed to have a new limit cycle with a smaller amplitude because of the increased damping. Furthermore, we note that the two nondimensional system responses are very similar because $\lambda\beta^2 = 100$ for the "stiff" case in Fig. 3(a) and $\lambda = 100$ for the "heavy" case in Fig. 3(b).

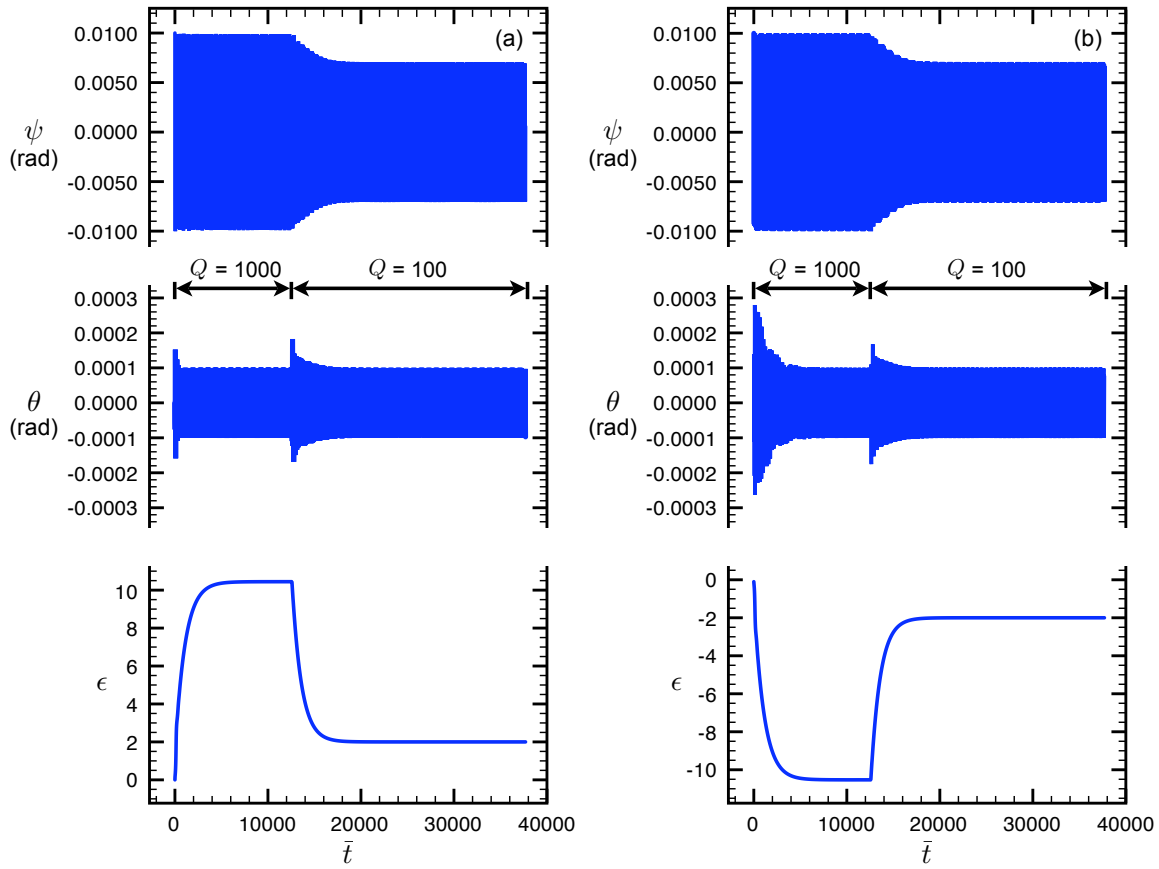

Figure 3: Response of the controlled system (Eqns. (11)) versus nondimensional time $\bar{t}$ with (a) $\beta = 10$ and $\lambda = 1$ or (b) $\beta = 0.1$ and $\lambda = 100$. The quality factor Q jumps from 1000 to 100 at $\bar{t} = 2000(2\pi)$. The other parameters used are $\zeta_\mathrm{a} = \zeta_\mathrm{s}$, $\alpha = 20000$, $\omega_\mathrm{f} = 0.05$, $\zeta_\mathrm{f} = 1$, and $\nu = 1000$. The three plots within a subfigure have the same abscissa seen at the bottom of the subfigure.

To understand how well the controlled system works, the nondimensional limit-cycle amplitudes A_θ and A_ψ are plotted in Fig. 4 along with their ratio A_ψ/A_θ as a function of the quality factor. As Q decreases from 1000 to 100 for the two

systems of Fig. 3, Fig. 4(a) reveals that A_θ changes by only about 0.25 %. In fact, A_θ can "jump" at most by about 0.4 %, and that maximum shift drops to about 0.1 % as the systems quadruple in "stiffness" ($\lambda\beta^2$) or "heaviness" (λ) for the systems of Fig. 4(b).

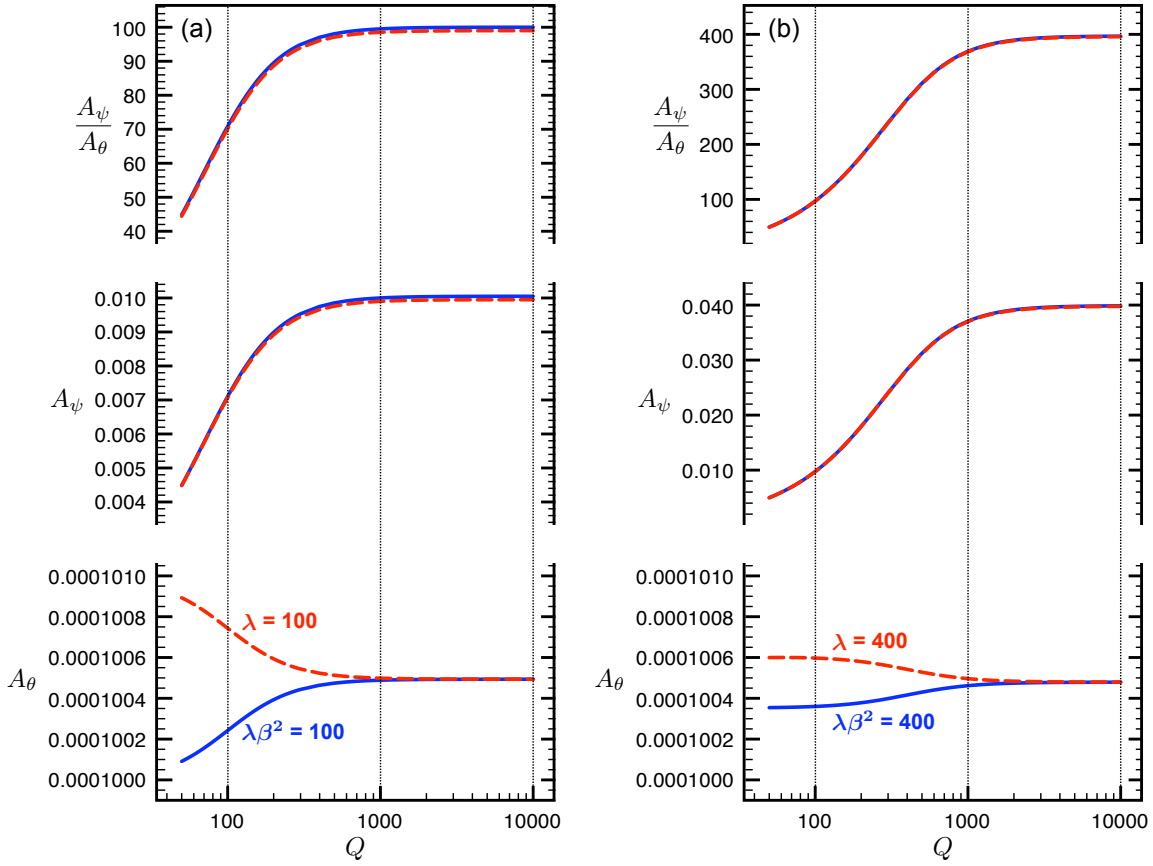

Figure 4: The nondimensional limit-cycle amplitudes A_θ and A_ψ along with their ratio A_ψ/A_θ as a function of the quality factor Q for the controlled system (Eqns. (11)) with (a) $\beta = 10$ and $\lambda = 1$ (solid curve) or $\beta = 0.1$ and $\lambda = 100$ (dashed curve), or (b) $\beta = 10$ and $\lambda = 4$ (solid curve) or $\beta = 0.1$ and $\lambda = 400$ (dashed curve). The parameter α was set to either (a) 20000 or (b) 12600 with $\zeta_\mathrm{a} = \zeta_\mathrm{s}$ and the 2nd-order filter being "perfect" ($\omega_\mathrm{f} \approx 0$). The three plots within a subfigure have the same abscissa seen at the bottom of the subfigure.

These results show that the oscillator could be calibrated as a velocity standard in air and used in ultra-high vacuum for a velocity shift within 0.4 %, at the worst. This is because the nondimensional frequency $\bar{\omega}$ changes insignificantly with Q, while the amplitude A_θ changes only slightly with Q, as seen in Fig. 4, resulting in a maximum velocity $\bar{\omega}A_\theta$ that changes only slightly with Q.

Microfabrication

Because the nondimensional system is successfully controlled, the dimensional system should likewise be controlled. Consequently, five microdevices were created with the same fundamental design shown in Fig. 1(a) but with different planform dimensions. The physical parameters were chosen to maximize the sensing current while keeping the limit-cycle frequencies between 50 kHz and 200 kHz and the overall micro-oscillator length less than 2 mm. For limit-cycle amplitudes of 1 nm at point P in Fig. 1(a), the five devices have theoretical sensing current amplitudes on the order of 1 μA in air or vacuum.

The microdevices were fabricated from a double-stack silicon-on-insulator (SOI) wafer with the following dimensions (from wafer top to bottom): 30 μm device layer, 200 nm oxide layer, 5 μm device layer, 2 μm oxide layer, and a 400 μm handle. The main microfabrication steps are outlined in Fig. 5, with each step involving a different photomask. As seen

in Fig. 5, SiO_2 is deposited first to act as an insulator between the top device layer and the conductive microwires, in order to prevent significant losses in the inductances of the microcoils due to current leakage through the substrate [16]. Second, a thin layer of chromium is deposited on top of the SiO_2 to act as an interface for the subsequent gold deposition for the microwires. The resulting chrome/gold microwires have transverse cross-sectional dimensions of about 10 μm width and 2.5 μm height. Next, nickel is deposited as the magnetic thin film (3rd step) with a thickness of at least 1 μm. Deep reactive-ion etching (DRIE) is then used to make the thin flexure (4th step) and form the planform geometry of the device (5th step), resulting in a gap width of about 5 μm. Finally, DRIE is used to etch the backside of the device and a buffered oxide etch is used to free the device.

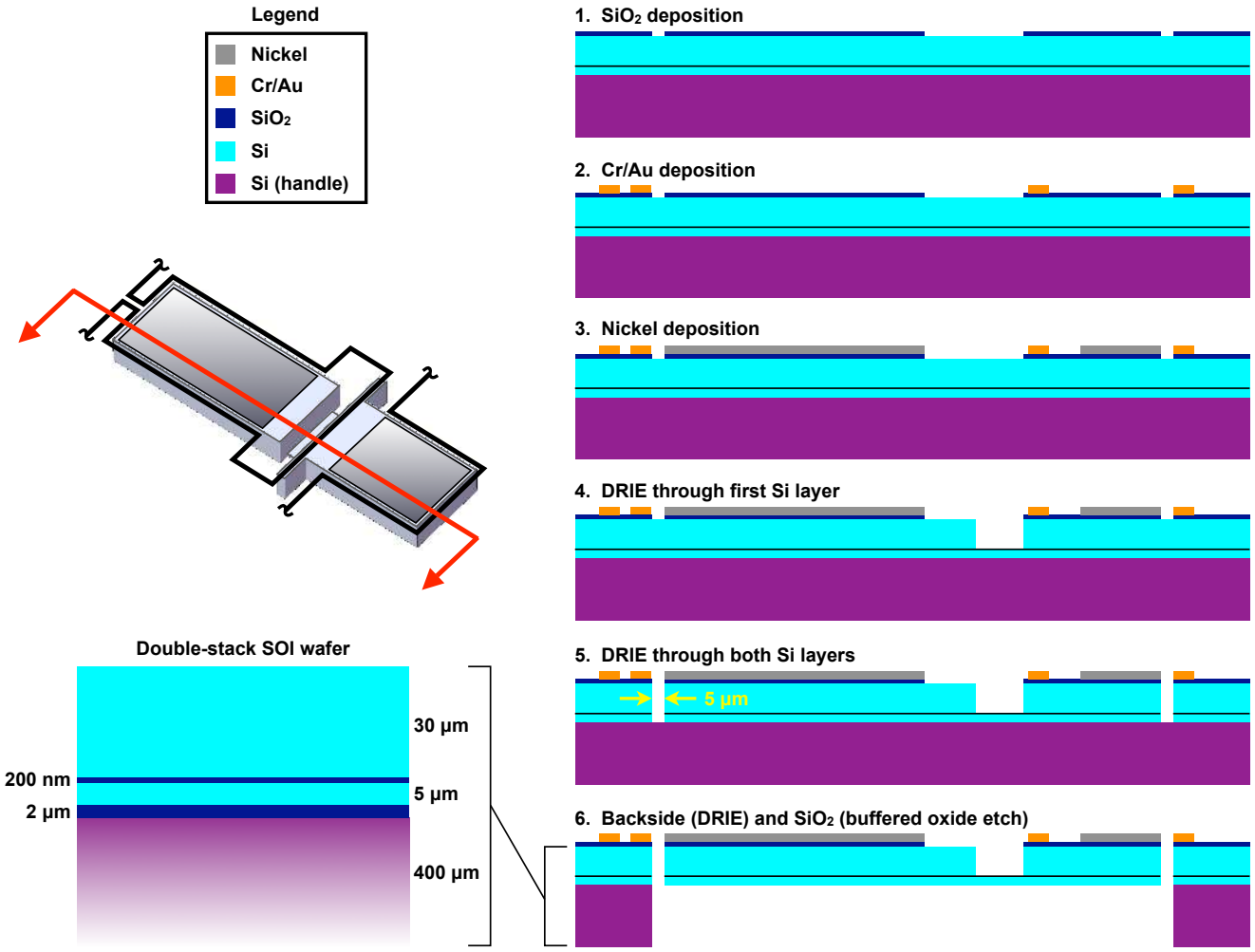

Figure 5: Main steps for microfabrication of each micro-oscillator.

The present use of magnetic thin films and microwires for sensing/actuation is in line with previous research. For example, AFM cantilevers [17, 18] and micro-oscillators coated in thin films like cobalt [19], nickel [20], or Permalloy [21] have been magnetically actuated to resonance. Magnetic thin films were also used for sensing or as passive elements in MEMS [22–24]. Furthermore, most microwires that are fabricated into microcoils are composed of non-magnetic metallic substances like gold [25, 26], copper [27], or aluminum [28] and carry currents to influence or sense the motion of nearby magnets.

However, the microdevices presented in this paper were developed completely with standard microfabrication processes, in contrast with some previous devices. Specifically, some researchers have glued micrometer-sized magnets onto AFM cantilevers [29–32], attached sharpened magnetic wires onto quartz tuning forks [33], or placed macroscale magnets in

devices [34]. Thus, the current work is another step towards the integration of microfabrication processes for magnetic sensing and actuation.

Conclusions

A new self-excited micro-oscillator based on magnetic sensing and actuation was developed as a velocity standard for use in the measurement of SI-traceable nanonewton-level forces. Five silicon-based oscillators with unique planform geometries were microfabricated with thin films of nickel that are closely surrounded by chrome/gold microwires. The sensing current is governed by Faraday's law of magnetic induction, and when that current is amplified to produce the actuation current, a magnetically-induced torque on the actuation side ensues. A novel analog control scheme controls the gain in order to yield a nanometer-level oscillation of the actuation side that is fairly insensitive to the quality factor. Theoretically, it was shown that the micro-oscillators could be calibrated as velocity standards in air and then used in ultra-high vacuum with velocity shifts within about 0.4 %. Future tests will hopefully confirm that the actuation sides of the devices oscillate with velocities that are independent of the surrounding air or vacuum.

The micro-oscillators will be used to calibrate AFM cantilevers by means of SI-traceable electrostatic nanonewton-level forces according to standards of the National Institute of Standards and Technology (NIST). Because every device is unique in geometry and expected to be unique in velocity, the accuracy of the non-contact calibration method might be determined by using all the devices to calibrate the same AFM cantilever. Therefore, not only is the microdevice another step towards the integration of microfabrication processes for magnetic sensing and actuation, but it is also a potential means to transform AFM cantilevers into force transducers for fundamental metrology of electrical and mechanical nanoscale quantities.

Acknowledgments

Thanks go to John Kramar (Manufacturing Engineering Laboratory) as well as Alex Liddle and Jason Crain (Center for Nanoscale Science and Technology) at NIST for their constructive advice towards this work. Many thanks also go to NIST and the National Research Council (NRC) for sponsoring Gregory W. Vogl as a postdoctoral research associate.

References

[1] Binnig, G., Quate, C. F., and Gerber, Ch. "Atomic force microscope". *Physical Review Letters,* **56**(9), pp. 930–933, 1986.

[2] Giessibl, F. J. "Atomic resolution of the silicon (111)-(7×7) surface by atomic force microscopy". *Science,* **New Series, 267**(5194), pp. 68–71, 1995.

[3] Kitamura, S., and Iwatsuki, M. "Observation of 7×7 reconstructed structure on the silicon (111) surface using ultrahigh vacuum noncontact atomic force microscopy". *Japanese Journal of Applied Physics,* **34**(2(1B)), pp. L145–L148, 1995.

[4] Cross, B., Ronzon, F., Roux, B., and Rieu, J.-P. "Measurement of the anchorage force between GPI-anchored alkaline phosphatase and supported membranes by AFM force spectroscopy". *Langmuir,* **21**, pp. 5149–5153, 2005.

[5] Sonnenberg, L., Parvole, J., Borisov, O., Billon, L., Gaub, H. E., and Seitz, M. "AFM-based single molecule force spectroscopy of end-grafted poly(acrylic acid) monolayers". *Macromolecules,* **39**, pp. 281–288, 2006.

[6] Hutter, J. L., and Bechhoefer, J. "Calibration of atomic-force microscope tips". *Review of Scientific Instruments,* **64**(7), pp. 1868–1873, 1993.

[7] Butt, H.-J., and Jaschke, M. "Calculation of thermal noise in atomic force microscopy". *Nanotechnology,* **6**(1), pp. 1–7, 1995.

[8] Cleveland, J. P., Manne, S., Bocek, D., and Hansma, P. K. "A nondestructive method for determining the spring constant of cantilevers for scanning force microscopy". *Review of Scientific Instruments,* **64**(2), pp. 403–405, 1993.

[9] Sader, J. E., Larson, I., Mulvaney, P., and White, L. R. "Method for the calibration of atomic force microscope cantilevers". *Review of Scientific Instruments,* **66**, pp. 3789–3798, 1995.

[10] Koch, S. J., Thayer, G. E., Corwin, A. D., and de Boer, M. P. "Micromachined piconewton force sensor for biophysics investigations". *Applied Physics Letters,* **89**, pp. 173901–1–173901–3, 2006.

[11] Gates, R. S., and Pratt, J. R. "Prototype cantilevers for SI-traceable nanonewton force calibration". *Measurement Science and Technology,* **17**, pp. 2852–2860, 2006.

[12] Pratt, J. R., Kramar, J. A., Newell, D. B., and Smith, D. T. "Review of SI traceable force metrology for instrumented indentation and atomic force microscopy". *Measurement Science and Technology,* **16**, pp. 2129–2137, 2005.

[13] Cumpson, P. J., and Hedley, J. "Accurate analytical measurements in the atomic force microscope: a microfabricated spring constant standard potentially traceable to the SI". *Nanotechnology,* **14**, pp. 1279–1288, 2003.

[14] Chung, K.-H., Shaw, G. A., and Pratt, J. R. "Direct electrostatic calibration of hybrid sensors for small force measurement". In SEM Annual Conference and Exposition on Experimental and Applied Mechanics 2007, pp. 1262–1269, 2007.

[15] Vogl, G. W., and Pratt, J. R. "Development of a self-excited oscillator for quantitative measurements in atomic force microscopy". In 2008 Design Engineering Technical Conferences & Computers and Information in Engineering Conference. To be published, 2008.

[16] Coutrot, A.-L., Dufour-Gergam, E., Martincic, E., Gilles, J.-P., Grandchamp, J.-P., Quemper, J.-M., Bosseboeuf, A., Alves, F., and Ahamada, B. "Electromagnetic micro-device realized by electrochemical way". *Sensors and Actuators A: Physical,* **91**, pp. 80–84, 2001.

[17] Han, W., Lindsay, S. M., and Jing, T. "A magnetically driven oscillating probe microscope for operation in liquids". *Applied Physics Letters,* **69**(26), pp. 4111–4113, 1996.

[18] Body, C., Reyne, G., Meunier, G., Quandt, E., and Seemann, K. "Application of magnetostrictive thin films for microdevices". *IEEE Transactions on Magnetics,* **33**(2), pp. 2163–2166, 1997.

[19] Beyder, A., and Sachs, F. "Microfabricated torsion levers optimized for low force and high-frequency operation in fluids". *Ultramicroscopy,* **106**, pp. 838–846, 2006.

[20] Grigore, L., Ensell, G., and Evans, A. "Microfabrication of sensors with magnetic resonating elements for further application in molecular probe chemistry". *Sensors and Actuators A: Physical,* **123–124**, pp. 285–289, 2005.

[21] Min, D. H., and Moreland, J. "Quantitative measurement of magnetic moments with a torsional resonator: Proposal for an ultralow moment reference material". *Journal of Applied Physics,* **97**, pp. 10R504–1–10R504–3, 2005.

[22] Castellana, C., Giazotto, F., Governale, M., Taddei, F., and Beltram, F. "Superconductor-semiconductor magnetic microswitch". *Applied Physics Letters,* **88**, pp. 052502–1–052502–3, 2006.

[23] Perez, L., Aroca, C., Sánchez, P., López, E., and Sánchez, M. C. "Planar fluxgate sensor with an electrodeposited amorphous core". *Sensors and Actuators A: Physical,* **109**, pp. 208–211, 2004.

[24] Chiriac, H., Pletea, M., and Hristoforou, E. "Magneto-surface-acoustic waves microdevice using thin film technology: design and fabrication process". *Sensors and Actuators A: Physical,* **91**, pp. 107–111, 2001.

[25] Wagner, B., and Benecke, W. "Microfabricated actuator with moving permanent magnet". In Proceedings of IEEE Micro Electro Mechanical Systems (MEMS '91), pp. 27–32, 1991.

[26] Koukharenko, E., Moktadir, Z., Kraft, M., Abdelsalam, M. E., Bagnall, D. M., Valeb, C., Jones, M. P. A., and Hinds, E. A. "Microfabrication of gold wires for atom guides". *Sensors and Actuators A: Physical,* **115**, pp. 600–607, 2004.

[27] Ramadan, Q., Samper, V., Poenar, D., and Yu, C. "Magnetic-based microfluidic platform for biomolecular separation". *Biomed Microdevices,* **8**, pp. 151–158, 2006.

[28] Hirota, T., Siraiwa, T., Hiramoto, K., and Ishihara, M. "Development of micro-coil sensor for measuring magnetic field leakage". *Japanese Journal of Applied Physics,* **32**(1(7)), pp. 3328–3329, 1993.

[29] Jarvis, S. P., Dürig, U., Lantz, M., Yamada, H., and Tokumoto, H. "Feedback stabilized force-sensors: a gateway to the direct measurement of interaction potentials". *Applied Physics A,* **66**, pp. S211–S213, 1998.

[30] Jarvis, S. P., Tokumoto, H., Yamada, H., Kobayashi, K., and Toda, A. "Alternative method for the activation and measurement of lateral forces using magnetically controlled atomic force microscopy". *Applied Physics Letters,* **75**(24), pp. 3883–3885, 1999.

[31] Kageshima, M., Takeda, S., Ptak, A., Nakamura, C., Jarvis, S. P., Tokumoto, H., and Miyake, J. "Measurement of intramolecular energy dissipation and stiffness of a single peptide molecule by magnetically modulated atomic force microscopy". *Japanese Journal of Applied Physics,* **43**(12A), pp. L1510–L1513, 2004.

[32] Higgins, M. J., Riener, C. K., Uchihashi, T., Sader, J. E., McKendry, R., and Jarvis, S. P. "Frequency modulation atomic force microscopy: a dynamic measurement technique for biological systems". *Nanotechnology,* **16**(3), pp. S85–S89, 2005.

[33] Todorovic, M., and Schultz, S. "Magnetic force microscopy using nonoptical piezoelectric quartz tuning fork detection design with applications to magnetic recording studies". *Journal of Applied Physics,* **83**(11), pp. 6229–6231, 1998.

[34] Ohashi, T., Kuyama, H., Hanafusa, N., and Togawa, Y. "A simple device using magnetic transportation for droplet-based PCR". *Biomed Microdevices,* **9**, pp. 695–702, 2007.